Isolating the Effect of Geometric Porosity on Supersonic Mars Parachute Drag: A Controlled CFD Investigation Using Historical Mission Porosities

Aaditya Manjith

Institution Royal Grammar School, Newcastle

Abstract

Introduction: Mars parachutes must operate at supersonic speeds, and past missions have used different canopy designs and porosities. Their aerodynamic results were obtained under different test conditions and numerical methods, so the effect of porosity alone cannot be determined from the reported drag coefficients. This study aims to determine how geometric porosity affects the drag coefficient and flow field of a supersonic disk-gap-band (DGB) parachute, using computational fluid dynamics (CFD) with all other conditions held constant.

Methods: A three-dimensional, 48-rib DGB canopy based on the Viking 1 profile was built in Autodesk Fusion 360. Only the annular gap was changed, to give porosities of 9.3%, 10%, 12.5%, 15% and 22.4 (corresponding to past Mars missions). Steady-state compressible Reynolds-averaged Navier–Stokes simulations with the k- SST turbulence model were run in Autodesk CFD at 450 m/s (approximately Mach 2) and 230 K, with a gas constant appropriate for a CO -dominated atmosphere. The mesh procedure, domain and number of iterations (200) were the same for every configuration. Drag coefficient was regressed against porosity (n = 5).

Results: The uncompensated drag coefficient decreased from 5.935 at 9.3% porosity to 5.518 at 22.4%, a reduction of about 7.03%. The largest drop occurred between 12.5% and 15%, and the change between 10% and 12.5% was comparatively small. The negative correlation was statistically significant ($r = -0.890$, p 0.043). Contours showed high pressure ahead of the canopy, and in all configurations a low-velocity separated wake with reverse flow and a total-pressure deficit. The extent and structure of these features varied with porosity.

Discussion: Porosity measurably influences drag and wake structure, and its effect appears to extend beyond the reduction in projected solid area. Comparing historical parachutes on porosity alone may therefore be misleading. The results differ from earlier NASA experiments, which found little porosity effect. This may be because those models were deployed behind a forebody and moved during testing, whereas the present canopy was isolated and fixed. The study has no mesh-independence analysis, uses steady RANS, and depends on the reference-area definition, so the results are not quantitatively validated. Future work should establish mesh independence and turbulence-model sensitivity, examine domain blockage, reconstruct Pathfinder, Viking and Huygens geometries, and compare against experiments on a matching isolated canopy.

Introduction:

In order to deliver payloads to the surface of Mars, reliable entry, descent, and landing (EDL) systems are needed. The Martian atmosphere is thin, approximately 1% of Earth's atmospheric pressure (Leovy,1977), thus a spacecraft must use several methods to slow down before landing. Parachutes are an important part of this process because they provide aerodynamic deceleration after the spacecraft has passed through the initial hypersonic entry phase. They reduce the vehicle's speed so that other landing systems, such as airbags, retrorockets, or sky cranes, can operate safely. However, Mars parachutes are different from parachutes used on Earth atmosphere because they need to deploy and operate at supersonic speeds (Nelessen, 2019). This creates a highly compressible and separated flow around the canopy, making it important to predict the aerodynamic forces accurately when designing Mars landing systems.

The flow around a parachute is also much more complicated than the flow around a conventional streamlined body. A deployed canopy produces drag mainly because of the pressure difference between its front and rear surfaces. At the same time, air flows through and around the canopy, creating shear layers, recirculation regions, and a large wake behind it (Peterson, 1996). At supersonic speeds, shock waves also form, causing large changes in pressure, density, and temperature (Anderson, 2003). These effects occur together with turbulence, boundary-layer development, flow separation, and wake mixing (Peterson, 1996). As a result, predicting the drag of a supersonic parachute is a challenging computational fluid dynamics (CFD) problem.

One of the important geometric factors affecting parachute performance is canopy porosity. Porosity refers to the percentage of the projected canopy area that is made up of openings. These openings allow some of the flow to pass through the canopy. Changing the porosity can affect the pressure distribution over the canopy, the size and strength of the wake, and the overall drag coefficient (Maynard, 1961; Jiang et al., 2023). This is especially important when comparing different Mars parachute designs. For example, Mars parachute systems have used different canopy designs and porosities, including approximately 9.3% for Mars Pathfinder (Xu, 2024), approximately 12.5% for Viking and similar hemisflo parachutes (Maynard, 1961), and approximately 22.4% for the Huygens parachute system (Lingard, 1995). However, the aerodynamic results for these parachutes were obtained using different test conditions and numerical methods.

Because of these differences, it is difficult to compare the reported drag coefficients from different Mars parachute programmes directly. Changes in aerodynamic performance may be caused by porosity, but they may also be caused by differences in canopy shape, payload or forebody geometry, wake interaction, wind-tunnel conditions, flow properties, computational mesh, solver, or turbulence model (Cruz et al., 2003). For example, a parachute located behind a spacecraft forebody will experience a different flow field from an isolated parachute placed in a uniform free stream. Therefore, although previous studies provide useful information, they cannot be used on their own to determine the effect of porosity accurately.

CFD can help overcome this problem because it allows individual parameters to be changed while keeping the other conditions the same. This makes it possible to study the effect of porosity in a more controlled way. Reynolds-averaged Navier–Stokes (RANS) turbulence models are commonly used because they provide a practical way of modelling turbulent flows without requiring excessive computational resources (Menter, 1994).

This study investigates the effect of geometric porosity on the aerodynamic performance of a supersonic disk-gap-band (DGB) parachute using computational fluid dynamics. A 3-dimentional model of a Mars-relevant DGB parachute is simulated under uniform Mach 2.0 flow, with the canopy geometry and flow conditions held constant while geometric porosity is systematically varied. Five porosity configurations are investigated: 9.3%, 10%, 12.5%, 15%, and 22.4%. The 10%, 12.5%, and 15% configurations correspond to the porosity range investigated in historical NASA experiments (Maynard, 1961), while the 9.3% and 22.4% configurations extend the investigation to porosity values representative of other Mars parachute systems (Xu, 2024 and Lingard, 1995).

The study aims to determine how geometric porosity affects the aerodynamic drag coefficient and the associated flow field. In addition to the calculated drag coefficient, velocity, streamwise velocity, static-pressure, and total-pressure fields are examined to investigate changes in the separated wake and pressure distribution with porosity. The investigation therefore focuses primarily on the relative effect of porosity under otherwise identical computational conditions.

Methods:

Reference geometry:

Defining geometric porosity:

Geometric porosity is an important parameter that describes the proportion of the projected canopy area with openings through which the surrounding flow can pass through. For this axisymmetric

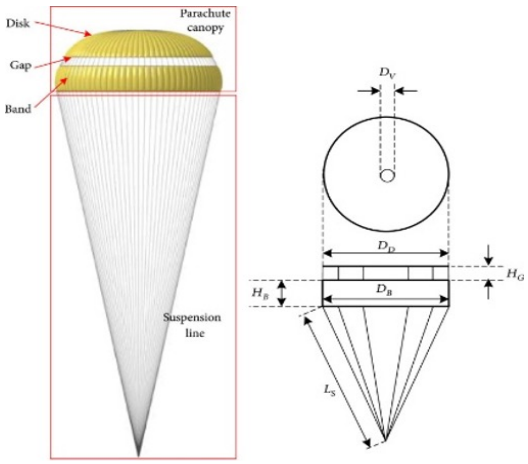

(a) DGB Parachute diagram of Viking 1



(b) 3D model of DGB parachute used in CFD testing

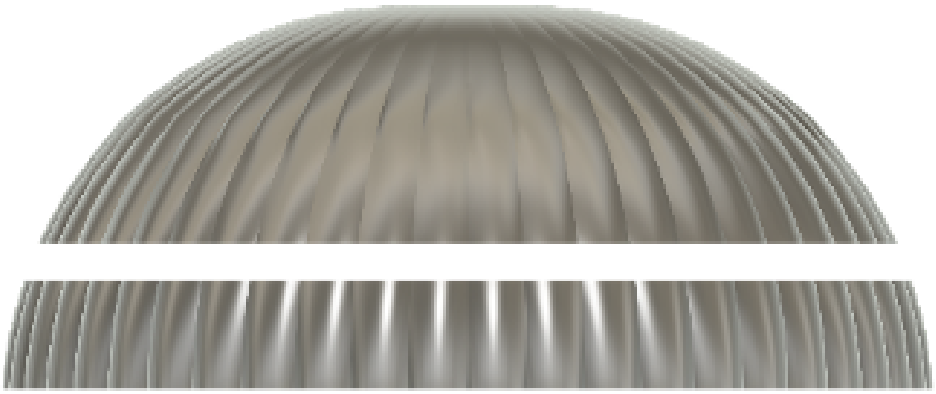

(c) Side view of DGB

Figure 1: DGB parachute diagram and reconstructed geometry. (a) Reference parachute diagram; (b) three-dimensional model used in the CFD investigation; (c) side view of the DGB canopy. Source of reference diagram: Huang et al. (2022).

DGB parachute, porosity is introduced through the annular gap between the disk and band (Fig 1). The porosity of the parachute is defined as:

$$\phi = \frac{A_{open}}{A_{ref}}$$

Where A_{open} is the total area of the openings in the canopy, and A_{ref} is the projected reference area of the canopy. For this circular canopy, it is given by

$$A_{ref} = \frac{\pi {D_0}^2}{4}$$

Where D_0 is the nominal parachute diameter.

The annular gap was iteratively adjusted in Fusion 360 until the calculated projected open area corresponded to the target porosity. This procedure generated five geometrically consistent parachute

configurations differing only in geometric porosity.

Modeling of the parachutes and changing porosities:

The reference DGB profile, from the Viking 1 program, was reconstructed in Autodesk Fusion 360 v.2605.0.97 using the published geometric dimensions of the selected reference configuration. The canopy was modelled as a three-dimensional ribbed surface comprising of a central disk, annular gap and outer band, with the nominal canopy diameter D_0 used as the principal geometric scale, of which all other dimensions were scaled from. The dimensions of the disk, gap and band profile were maintained across all simulations. The canopy was designed from a two-dimensional radial cross-section defining the canopy profile. A single rib surface was constructed using the prescribed radial dimensions and was then replicated circumferentially using a circular pattern to produce 48 equally spaced ribs. The outer portion of the rib profile was defined using a circular arc with a specified radius and centre, allowing the curvature of the canopy edge to be controlled independently of the remainder of the profile. The resulting surfaces were used to generate the three-dimensional DGB canopy geometry. The terminal canopy curvature was defined as a circular arc of radius $0.0375D_0$, centred at ($0.48D_0$, $0.03125D_0$) relative to the parachute centreline. For the parametric study, the rib profile and all canopy dimensions were held constant except for the geometry defining the annular gap. The gap was adjusted to produce target geometric porosities of 9.3%, 10%, 12.5%, 15% and 22.4%.

Physics equations:

The compressible flow was governed by the compressible Navier–Stokes equations, expressed through the conservation of mass, momentum and energy. These equations describe the conservation of mass, the balance of momentum resulting from pressure and viscous forces, and the conservation of energy within the flow (Anderson, 2003).

Conservation of mass:

$$\frac{\partial \rho}{\partial t} + \nabla \cdot (\rho \mathbf{u}) = 0$$

Conservation of momentum:

$$\frac{\partial (\rho \mathbf{u})}{\partial t} + \nabla \cdot (\rho \mathbf{u} \otimes \mathbf{u}) = -\nabla p + \nabla \cdot \tau$$

Conservation of energy:

$$\frac{\partial (\rho E)}{\partial t} + \nabla \cdot [(\rho E + p)\mathbf{u}] = \nabla \cdot (k \nabla T) + \nabla \cdot (\tau \cdot \mathbf{u})$$

Because the present simulations model a steady-state compressible supersonic flow, density, pressure and temperature are coupled and the energy equation is required to account for the thermodynamic changes associated with compression and expansion of the flow.

The simulations use a Reynolds-averaged Navier–Stokes (RANS) formulation to represent turbulence. In RANS, the instantaneous velocity is decomposed into a mean component and a fluctuating component:

$$u_i = \overline{u_i} + u_i'$$

where $\overline{u_i}$ is the mean velocity and u_i' is the turbulent fluctuation. Reynolds averaging introduces additional Reynolds-stress terms into the governing equations. These terms are not directly resolved by the RANS formulation and are instead modelled using a turbulence closure. In this study, the k-ω SST model was used to provide this closure (Menter, 1994).

We quantify the aerodynamic performance of the canopy using the drag coefficient, which is given by:

$$C_d = \frac{2F_d}{\rho_\infty v_\infty^2 A_{ref}}$$

Where C_d is the Coefficient of turbulent drag, F_d is the drag force experienced on the canopy, is the density of the fluid, A is the area of the canopy viewed from the direction of the fluid flow, and v is the flow velocity. The drag force is a result obtained through the CFD simulations, which, for this geometry, is mainly comprised of the pressure forces from the shocks.

CFD Setup:

A three-dimensional computational model of the DGB parachute was constructed using the geometric dimensions described previously. The parachute was positioned within a cylindrical computational domain representative of a wind-tunnel configuration. The domain diameter was set to approximately $4D_0$ where D_0 is the nominal parachute diameter, providing an approximately uniform radial clearance of $2D_0$ between the canopy centreline and the outer domain boundary. The inlet was located $4D_0$ upstream of the canopy, while the outlet was positioned $10D_0$ downstream. This provided sufficient upstream and downstream distance for development of the incoming flow and wake within the computational domain.

The simulations were performed under compressible flow conditions with a freestream velocity of 450 m/s, corresponding approximately to Mach 2 under the specified thermodynamic conditions. The freestream temperature was set to 230K with the working fluid represented using a specific gas constant of 188.9 J/K/Kg appropriate for a CO_2-dominated Martian atmosphere (Colozza and Jakupca, 2019). Density was treated as a dependent thermodynamic variable and determined by the compressible-flow solution.

Heat transfer was enabled and the advection scheme was set to ADV 5 (Modified Petrov–Galerkin), a more stable variation of the Petrov–Galerkin scheme implemented in Autodesk CFD (Autodesk, 2024). The simulations used Autodesk CFD's steady-state compressible solver with the k-ω Shear Stress Transport (SST) Reynolds-averaged Navier–Stokes (RANS) turbulence model. This turbulence model was retained for all porosity configurations to ensure that changes in the predicted aerodynamic behaviour arose from the prescribed geometric variation rather than from changes in computational turbulence.

At the inlet boundary, a velocity boundary condition of magnitude 450 m/s was applied in the direction normal to the incoming flow and towards the parachute. The downstream outlet was assigned a gauge pressure of 0 Pa. The remaining domain boundaries were treated according to Autodesk CFD flow-domain boundary conditions appropriate to the cylindrical wind-tunnel configuration.

The computational mesh was generated using the automatic meshing functionality within Autodesk CFD. The same meshing procedure and domain construction were maintained for each porosity configuration. Each simulation was advanced for 200 steady-state iterations, after which the aerodynamic forces and flow-field quantities were recorded. As the solver convergence criterion used internally by Autodesk CFD was not recorded, the 200-iteration solution was used consistently for all porosity configurations.

Turbulence models:

A single RANS turbulence model was used consistently for all simulations to isolate the effect of geometric porosity. The k-ω SST model was selected based on its availability within Autodesk CFD and its suitability for separated external aerodynamic flows (Menter, 1994). The same turbulence closure was retained for every porosity configuration so that differences in the predicted aerodynamic behaviour arose from the prescribed geometric variation rather than changes in the turbulence model.

Results:

Linear regression was performed via ordinary least squares (scipy.stats.linregress) to characterize the relationship between porosity (ϕ, independent variable) and drag coefficient (Cd, dependent variable)

for both compensated and uncompensated configurations (n = 5 per condition) (Fig 2) (Virtanen et al., 2020). Goodness of fit was assessed using the coefficient of determination (R^2) and Pearson correlation coefficient (r); statistical significance of the slope was evaluated via a two-tailed t-test (= 0.05), yielding the reported p-values. Standard error of the slope estimate was also computed to quantify uncertainty in the fitted relationship.

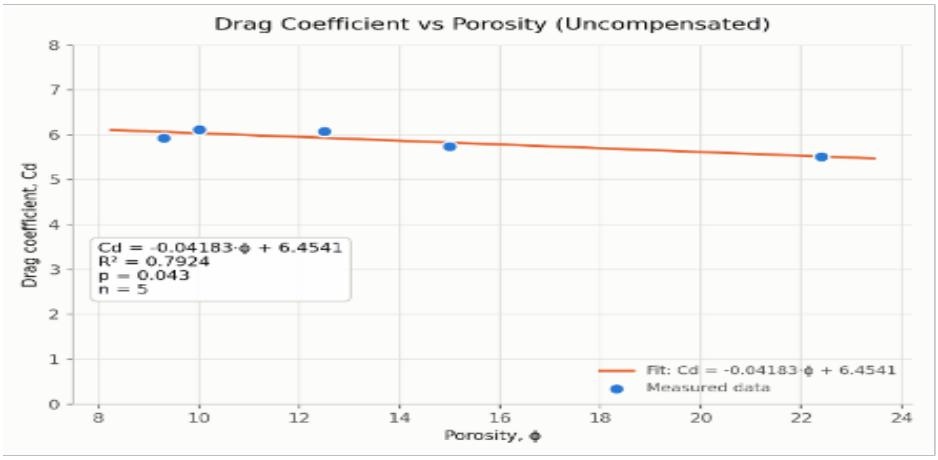

(a) Graph of C_d against posority for reference-area-uncompensated drag values

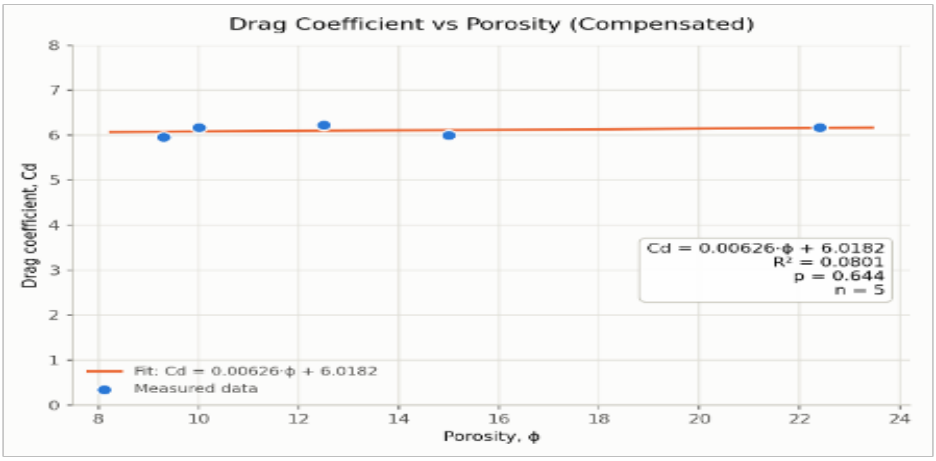

(b) Graph of C_d against posority for reference-area-compensated drag values

Figure 2: Plot of drag coefficient against porosity for the parachutes. A Pearson product-moment correlation coefficient (r) was calculated to investigate this relationship. For the five tests in the sample, the calculated value was *r=-0.890*. At a 5% significance level for a two-tailed test, the critical value for *n=5* was $r_{critical}$*=0.8783*. Since $|r| = 0.890 > 0.8783$, the null hypothesis (H_0) was rejected. Therefore, the data provides sufficient statistical evidence of a significant linear correlation between geometric porosity and drag coefficient.

The calculated drag coefficient generally decreased with increasing geometric porosity. The uncompensated drag coefficient decreased from 5.935 at 9.3% porosity to 5.518 at 22.4%, representing a reduction of approximately 7.03%. The largest reduction occurred between 12.5% and 15% porosity, while the change between 10% and 12.5% was comparatively small.

To investigate the aerodynamic mechanisms underlying this variation, velocity and pressure fields were examined for each porosity configuration.

1. Static pressure contours:

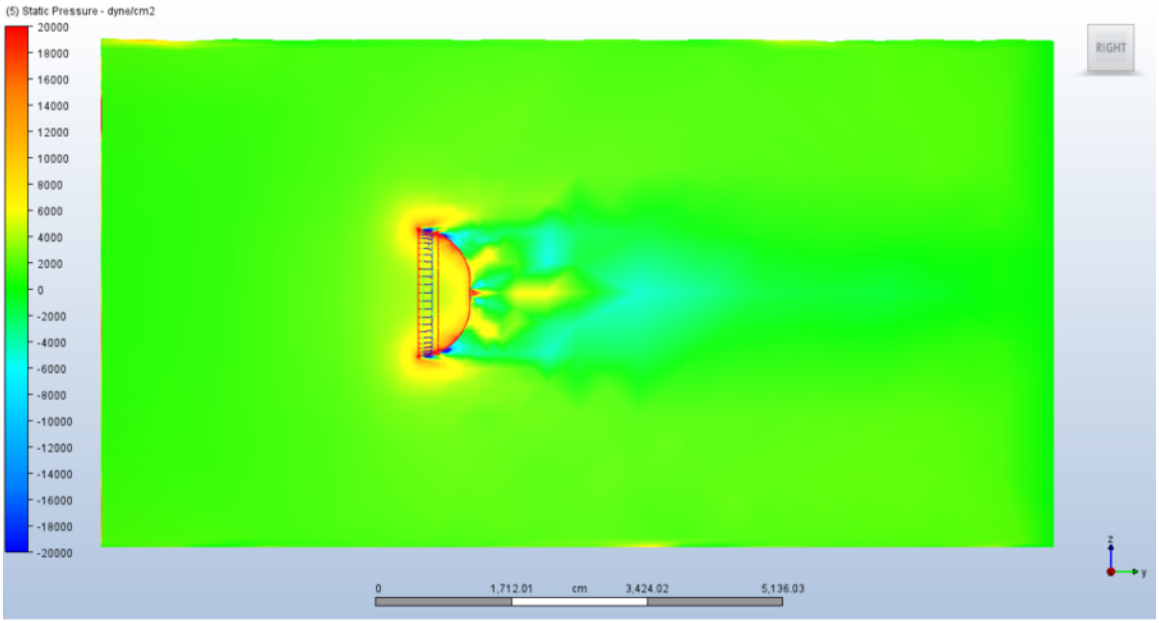

Figure 3: Static pressure plot of 10% porosity.

The static pressure contours (fig 3) show an high pressure region immediately in front of the canopy, as shown by the yellow region. This indicates the immediate compression of the air as it encounters the canopy. This pressure deficit upstream and downstream of the canopy contributes to F_d. The cyan region downstream of the canopy coincides spatially with the separated wake observed in the velocity contours. It extends for a substantial region downstream, which corresponds to the wake seen in the velocity plots, where in the V_{mag} plot, it is the area of lower velocity, and in the V_y plot, the area where recirculation occurs. In the different plots, the magnitude, and spatial extent of the pressure disturbance varies with porosity. This variation can be quantified through using the coefficient of pressure C_p, where C_p is given by:

$$C_p = \frac{p - p_\infty}{\frac{1}{2}\rho_\infty V_\infty^2}$$

2. Velocity magnitude:

The velocity magnitude contours (Fig 4) show the formation of low-velocity wakes downstream of the canopy, which is present in all porosity configurations. The wake originates immediately downstream of the canopy and persists into the downstream flow. Changes in the size and structure of the low velocity region are visible as geometric porosity varies, particularly in the near-wake region surrounding the DGB structure.

The higher porosity configurations show greater penetration of the external flow through the disk-gap region, which produced a visibly different near-wake structure when compared to the lower porosity configurations.

3. V_y plots

In our CFD tests, the component of the velocity vector parallel to the freestream was labelled V_y, and these contours (Fig 5) showed the presence of reversed flow and recirculation in the near-wake region, with negative V_y occuring immediately downstream of the canopy. This indicates flow separation and the formation of a recirculating wake. The extent and intensity of the reverse-flow region varies with geometric porosity.

4. Total pressure: Taking total pressure plots (Fig 6) showed a region of reduced total pressure

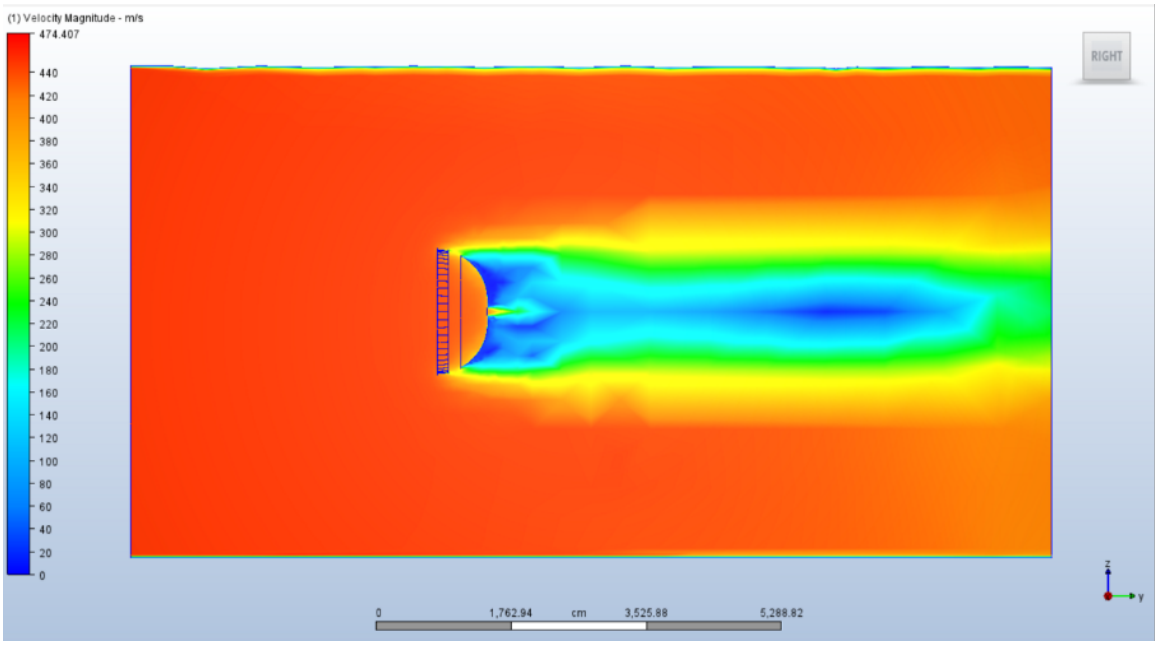

Figure 4: Velocity magnitude plot of 22.4% porosity.

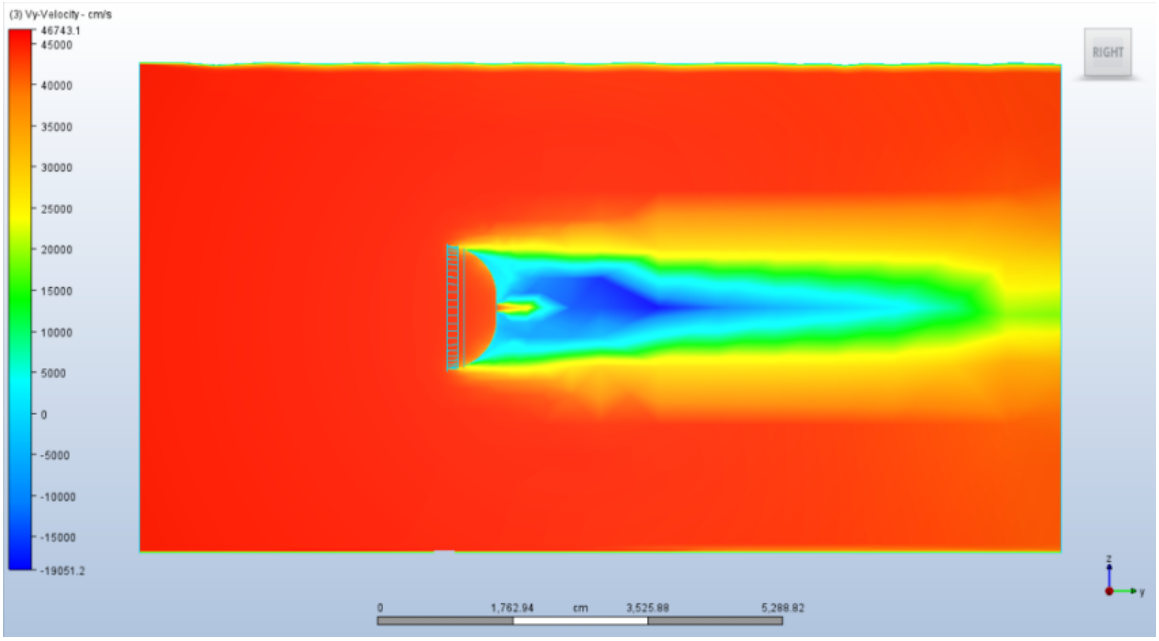

Figure 5: V_y plot of 12.5% porosity.

downstream of the canopy for all configurations. The total-pressure deficit is concentrated within the wake and is indicative of irreversible losses associated with shock formation, flow separation, and subsequent turbulent mixing. The spatial distribution of the total pressure deficit changes with geometric porosity.

Discussion:

This study investigated the effect of geometric porosity on the aerodynamic behaviour of a supersonic disk-gap-band Mars parachute using three-dimensional compressible CFD. Five porosity

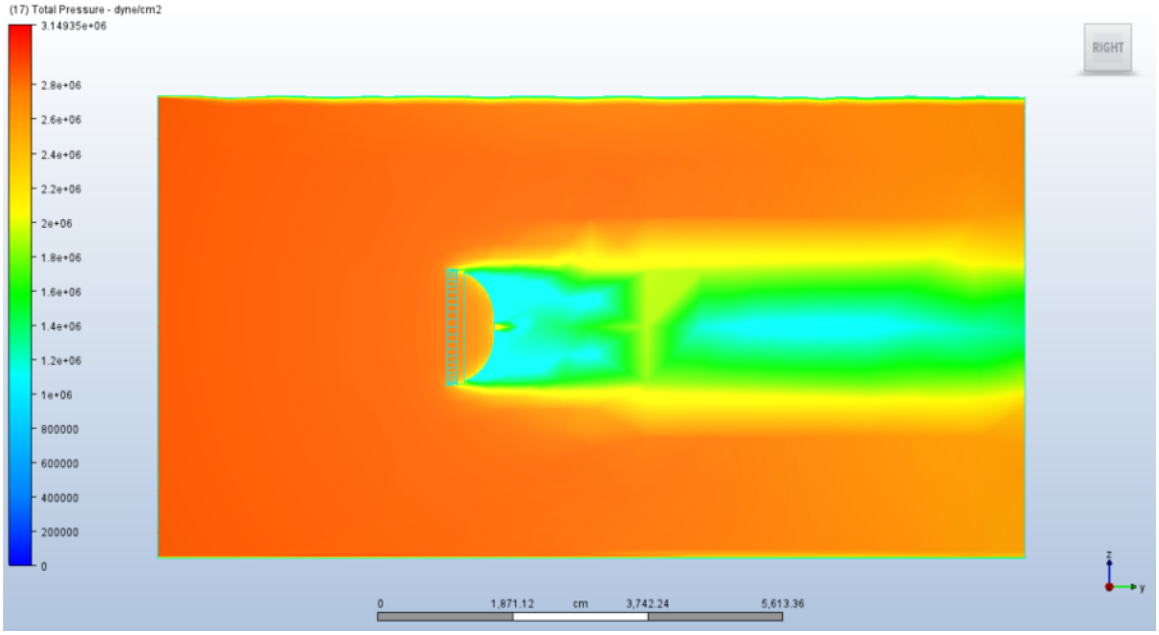

Figure 6: Total pressure plot of 15% porosity.

configurations, ranging from 9.3% to 22.4%, were investigated under otherwise consistent flow and computational conditions. The calculated drag coefficient generally decreased with increasing geometric porosity, indicating that porosity has a measurable influence on the aerodynamic performance of the canopy.

The results indicate that geometric porosity influences the aerodynamic behaviour of the supersonic DGB parachute, with the calculated drag coefficient generally decreasing as porosity increased. This reduction was accompanied by changes in the downstream wake, including variations in the extent of the reverse-flow region and the velocity deficit. Changes in the static and total pressure fields were also observed, indicating that the effect of porosity extends beyond the reduction in projected solid area and modifies the flow and pressure structure surrounding the canopy.

Across the investigated range of 9.3 -22.4% porosity, the uncompensated drag coefficient decreased from 5.935 to 5.518, corresponding to a reduction of approximately 7.0%. A statistically significant negative linear association was also obtained for the five configurations ($r = -0.890$, $p \approx 0.043$); however, this should be interpreted cautiously because of the small sample size and the limitations of the numerical model.

The present results differ from the experimental findings of Mayhue and Bobbitt, (1972 who investigated DGB parachutes with geometric porosities of 10%, 12.5% and 15% at Mach numbers between 2.0 and 3.0 and reported relatively little effect of geometric porosity on canopy inflation characteristics and drag within the tested range. In the present CFD simulations, increasing porosity was instead associated with a general reduction in calculated drag coefficient. This discrepancy may arise from differences between the experimental and numerical configurations rather than from porosity alone. The NASA models were deployed behind a forebody and exhibited canopy motion and changes in projected area, whereas the present model represents an isolated, fixed DGB canopy in a cylindrical computational domain. Consequently, the present simulations isolate geometric porosity more directly, but do not reproduce all the aerodynamic and structural characteristics of the experimental system.

This is consistent with later experimental comparisons of Viking and Mars Pathfinder DGB parachutes, which showed differences in measured drag even under comparable test conditions and identified factors including canopy geometry and fabric permeability as contributors to aerodynamic performance. The

controlled geometry used in the present study therefore provides a means of isolating the effect of geometric porosity from these additional parameters (Cruz et al., 2003).

The observed reduction in drag with increasing porosity may be associated with changes in the flow passing through the annular gap. Increasing the gap width provides a larger opening through which the incoming flow can pass, modifying the interaction between the internal flow and the separated wake downstream of the canopy. The V_y contours show negative streamwise velocity immediately downstream of the canopy, indicating the presence of a recirculating separated region. Variation in the axial extent of this reverse-flow region with porosity suggests that the disk-gap flow influences the structure of the downstream wake.

The velocity-magnitude contours similarly show a persistent velocity deficit downstream of the canopy for all porosity configurations, although the structure and spatial extent of the wake vary with porosity. The static-pressure contours show elevated pressure upstream of the canopy associated with deceleration and compression of the incoming flow, followed by a region of reduced pressure within the separated wake. Consequently, modifications to the wake produced by changes in porosity are accompanied by changes in the pressure field surrounding the canopy.

These pressure changes provide a possible mechanism for the observed variation in drag coefficient. Increasing porosity changes the flow through the canopy and therefore modifies the pressure distribution acting on its surfaces. Since pressure forces contribute directly to the aerodynamic drag, changes in this distribution can alter the resultant drag force. The total-pressure contours additionally show a pronounced pressure deficit within the wake, consistent with irreversible losses associated with shock formation, flow separation and turbulent mixing.

Although the overall relationship between porosity and drag was negative, the calculated drag coefficient did not decrease monotonically at every porosity increment. This behaviour may indicate that the aerodynamic response is not governed solely by the reduction in projected solid area. Instead, changes in gap flow and wake structure may produce competing effects on the pressure distribution. However, the observed deviations from monotonic behaviour should not be interpreted as physical effects with confidence until numerical and methodological sources of uncertainty, particularly mesh resolution, convergence and reference-area definition, have been assessed.

The study is subject to limitations associated with the numerical modelling, including the computational mesh, steady-state RANS treatment, and uncertainty in the reference-area definition. The definition of the reference area represents an important methodological consideration because geometric porosity changes the projected open area while the nominal canopy diameter remains constant. A consistent nominal reference area is therefore necessary when comparing \(C_D\) values between configurations. The mesh was generated using Autodesk CFD's automatic meshing procedure, and a formal mesh-independence study was not performed. Consequently, the sensitivity of the predicted drag coefficient and wake structure to spatial resolution remains uncertain. The use of a steady k-ω SST RANS formulation also limits the representation of the inherently unsteady separated wake. Large-scale turbulent structures and temporal fluctuations may therefore not be fully captured. The discrepancy between the calculated drag coefficients and published experimental values prevents the numerical model from being considered quantitatively validated. The NASA data are therefore treated as an external benchmark rather than as validation of the present CFD model.

The implication of this study is that porosity can affect supersonic parachute aerodynamics through changes in the flow field, and therefore comparisons of historical parachute systems based solely on their reported porosity values may be misleading. The results demonstrate the value of isolating geometric porosity in a controlled numerical environment. Historical Mars parachute programmes employed different canopy geometries and porosities, meaning that differences in their reported aerodynamic performance cannot necessarily be attributed to porosity alone. The present approach provides a controlled framework for examining this parameter independently.

Future work should first establish mesh independence and sensitivity to numerical convergence and turbulence modelling. The computational domain could also be systematically varied to quantify

blockage effects and determine their influence on the predicted drag. Further simulations using independently reconstructed Pathfinder, Viking and Huygens geometries would then allow the combined effects of porosity and canopy geometry to be separated. Experimental comparison using a matching isolated-canopy configuration would also provide a stronger basis for quantitative validation.

Conclusion:

This study investigated the effect of geometric porosity on the aerodynamic behaviour of a supersonic disk-gap-band parachute using three-dimensional compressible CFD. Across the investigated range of 9.3–22.4% porosity, the calculated drag coefficient generally decreased with increasing porosity. Examination of the velocity, streamwise velocity, static-pressure and total-pressure fields demonstrated that changing the annular gap modified the downstream separated wake and the pressure distribution surrounding the canopy. These results suggest that the influence of porosity extends beyond the reduction in projected solid area and involves changes in the flow structure through and downstream of the canopy.

The present CFD results differed from published experimental drag measurements, preventing quantitative validation of the numerical model. Nevertheless, the controlled variation of the annular gap provided an isolated investigation of geometric porosity under consistent computational conditions. The findings indicate that porosity is an important parameter in supersonic DGB parachute aerodynamics, while also demonstrating that differences between historical parachute programmes cannot necessarily be attributed to porosity alone. Further work incorporating mesh-independence studies, sensitivity to turbulence modelling and computational-domain dimensions, together with experimental validation using a matching isolated-canopy configuration, would strengthen the conclusions of the present investigation.

Bibliography

1. Leovy CB. The atmosphere of Mars. Scientific American. 1977 Jul 1;237(1):34-43.
2. Nelessen, A., Sackier, C., Clark, I., et al., "Mars 2020 Entry, Descent, and Landing System Overview," 2019 IEEE Aerospace Conference, Big Sky, MT, USA, 2019, pp. 1-20, doi: 10.1109/AERO.2019.8742167.
3. Peterson, C. W., Strickland, J. H., Higuchi, H. "The fluid dynamics of parachute inflation." *Annual Review of Fluid Mechanics* 28.1 (1996): 361-387.
4. Anderson, J.D. Modern Compressible Flow: with historical perspective. 3rd ed. McGraw-Hill
5. Jiang, L. et al. (2023). *Effect of Different Geometric Porosities on Aerodynamic Characteristics of Supersonic Parachutes*. Space: Science & Technology, 3, Article 0062. DOI: 10.34133/space.0062.
6. Xu X, Chen G, Zou T, Jia H, Rong W, Jiang W, Xue X. Numerical study on aerodynamic characteristics of Mars parachute system with different combinations of fabric permeability and structural porosity. Aerospace Science and Technology. 2024 Oct 1;153:109449.
7. Maynard JD. Aerodynamic characteristics of parachutes at Mach numbers from 1.6 to 3. National Aeronautics and Space Administration; 1961.
8. Lingard J, Underwood J. The effects of low density atmospheres on the aerodynamic coefficients of parachutes. In13th Aerodynamic Decelerator Systems Technology Conference 1995 May 15 (p. 1556).
9. Huang, M., Wang, W., & Li, J. (2022). *Analysis and Verification of Aerodynamic Characteristics of Tianwen-1 Mars Parachute*. Space: Science & Technology, 2022, Article 9805457. https://doi.org/10.34133/2022/9805457
10. Cruz et al. (2003), *Wind Tunnel Testing of Various Disk-Gap-Band Parachutes*.

11. Menter, F. R. (1994). *Two-Equation Eddy-Viscosity Turbulence Models for Engineering Applications*. AIAA Journal, 32(8), 1598–1605. DOI: 10.2514/3.12149.

12. Colozza, A. Jakupca, I. (2019) *Thermal System Sizing Comparison of a PEM and Solid Oxide Fuel Cell Systems on Mars*. NASA/TM—2019-220019. Cleveland, Ohio: National Aeronautics and Space Administration, Glenn Research Center.

13. Autodesk (2024) 'Advection Schemes', *Autodesk CFD User's Guide*. Available at: Autodesk CFD User's Guide – Advection Schemes (Accessed: 8 August 2026).

14. Virtanen, P. et al. (2020). *SciPy 1.0: Fundamental Algorithms for Scientific Computing in Python*. Nature Methods, 17, 261–272. DOI: 10.1038/s41592-019-0686-2.

15. Mayhue, Robert J., and Percy J. Bobbitt. *Drag characteristics of a disk-gap-band parachute with a nominal diameter of 1.65 meters at Mach numbers from 2.0 to 3.0*. No. L-8357. 1972.

Acknowledgement (for support and guidance)**-** Dr Unnikrishnan Nair S, Former director, Vikram Sarabhai Space Centre, India.